

Spin dynamics of the ferric wheel $\text{Fe}_6(\text{triethanolamine } 3\text{-})_6$ studied by electron and nuclear spin resonance

B. Pilawa,¹ R. Boffinger,¹ I. Keilhauer,¹ R. Leppin,¹ I. Odenwald,² W. Wendl,² C. Berthier,^{3,4} and M. Horvatic³

¹Physikalisches Institut, Universität Karlsruhe (TH), Wolfgang Gaede Strasse 1, 76128 Karlsruhe, Germany

²Kristall- und Materiallabor, Universität Karlsruhe (TH), Wolfgang Gaede Strasse 1, 76128 Karlsruhe, Germany

³Grenoble High Magnetic Field Laboratory, CNRS and MPI-FKF, Boîte Postale 166, 38042 Grenoble Cedex 9, France

⁴Laboratoire de Spectrométrie Physique, Université Joseph Fourier Grenoble I, 38402 St. Martin d'Hères, France

(Received 30 July 2004; revised manuscript received 24 February 2005; published 27 May 2005)

The dynamic properties of the cyclic hexanuclear iron(III) complex $\text{Fe}_6(\text{triethanolamine } 3\text{-})_6$ are studied by electron spin (ESR) and ^1H nuclear magnetic resonance. We analyze the angular and temperature dependence of the ESR absorption lines at 9.4 GHz in the magnetic field range up to 1 T, the temperature dependence of the ^1H longitudinal relaxation rate T_1^{-1} at 1.2 T, and the magnetic field dependence of T_1^{-1} between 12 and 17 T at 0.2, 1.5, and 5 K. The influence of the intermolecular dipolar interaction on the resonance properties of the $\text{Fe}_6(\text{triethanolamine } 3\text{-})_6$ complex is numerically calculated. The discussion of the experimental results indicates the importance of spin-lattice relaxation processes for the understanding of the dynamics of the iron ring.

DOI: 10.1103/PhysRevB.71.184419

PACS number(s): 75.50.Xx, 76.30.-v, 76.60.-k

I. INTRODUCTION

Cyclic polynuclear iron(III) complexes realize molecular rings of antiferromagnetically coupled spins $s=5/2$. The static magnetic properties of these rings resemble those of infinite spin chains. The static magnetic susceptibility is determined by the exchange coupling J of the spin-5/2 ions and follows the temperature dependence expected for infinite spin-5/2 antiferromagnetic Heisenberg chains,¹ provided that the temperature is high enough to hide the discrete energy level structure of the finite spin system due to thermal excitations. The dynamic properties of cyclic polynuclear metal complexes have been studied by Mössbauer spectroscopy,² inelastic neutron scattering,³ and nuclear magnetic resonance techniques.⁴ The detailed measurements of the nuclear spin relaxation of the protons surrounding the iron(III) ions of Lascialfari *et al.*⁴ showed that the longitudinal relaxation is characterized by a peak of the T_1^{-1} rate in the temperature range around $T \approx 30$ K and a linear increase for $T \geq 100$ K.^{4(a)} The peak was attributed to the special contribution of the first excited $S=1$ state and reflects the discrete energy level structure of the finite spin system whereas the T_1^{-1} rate at high temperatures reflects the quasicontinuum of the large number of excited spin states. For an overview of recent NMR results and further dynamics properties of cyclic polynuclear iron(III) complexes see Ref. 5.

The dynamic properties of antiferromagnetically coupled molecular ring systems attracted also considerable theoretical interest. It was shown that the dynamics of the Néel vector $\vec{n} \propto \sum_{i=1}^N (-1)^i \vec{s}_i$ is characterized by quantum rotations for low magnetic anisotropy and by coherent quantum tunneling if the magnetic anisotropy is large enough.⁶ The conditions for the existence of macroscopic quantum coherence in molecular magnetic rings were determined by semiclassical and exact diagonalization techniques,⁶⁻⁸ and it is only very recently that the phenomenon was observed by inelastic neutron scattering.⁹ For symmetry reasons electron spin reso-

nance (ESR) experiments are sensitive to the dynamics of the total spin but not to the motion of $n(t)$.^{6(b)} As far as NMR is concerned, the correlation function of $n(t)$ should in principle, in the close vicinity of the level crossings, affect the relaxation rate T_1^{-1} and even the line shape, with the appearance of satellite lines, provided the tunneling is coherent enough.⁸ Only an analysis of T_1 seems to be a viable experimental approach to $n(t)$, since the satellite lines are probably unobservable in a NMR experiment. The spin-spin relaxation rate (T_2^{-1}) of these lines is expected to be of the order of the decoherence rate (a few millikelvins), by far too fast (i.e., T_2 is too short) to allow a pulsed NMR signal detection. Even if we could *a priori* detect the signal by doing a continuous-wave NMR, the corresponding linewidth (0.1–1 GHz) would be too broad to allow any realistic recording of the spectrum.

In this paper we will discuss the spin dynamics of the iron(III) ring as it can be observed by ESR and NMR experiments, and we will point out the mutual relation between the results obtained by ESR and NMR experiments. The spin dynamics is determined by the intramolecular exchange interaction, the on-site anisotropy of the iron(III) spin, and the intramolecular dipolar interaction. These interactions determine essentially the energy level structure of the spin states of the iron(III) ring. Their magnitudes can be fixed by magnetization measurements in high magnetic fields,¹⁰ neutron scattering,¹¹ or ESR measurements.¹² The finite width of the ESR absorption lines indicates that also intermolecular and spin-phonon interactions have to be considered. The intermolecular dipolar coupling is determined by the crystal structure and can be used to calculate the temperature and magnetic field dependence of the nuclear spin-lattice relaxation T_1^{-1} rate, as well as the properties of the ESR lines. The calculation provides a quantitative basis for the discussion of the experimental results and reveals the crucial importance of spin-lattice relaxation processes.

The spin cluster $\text{Fe}_6(\text{triethanolamine } 3\text{-})_6$ [$\text{Fe}_6(\text{tea})_6$] is chosen as the model compound.¹³ The crystals form hexago-

nal prisms which can easily be oriented and the static magnetic susceptibility as well as ESR measurements^{12a,12b} characterize $\text{Fe}_6(\text{tea})_6$ as an ideal hexagonal ring system. The properties of $\text{Fe}_6(\text{tea})_6$ are explained in Sec. II together with details of the ESR and NMR techniques. Section III reports the experimental results. Section III A shows the ESR measurements at the microwave frequency of 9.44 GHz, in the magnetic field range up to 1 T. Section III B presents the ^1H NMR results, which were measured at 1.2 T (^1H Larmor frequency of 52 MHz) and, at the Grenoble High Magnetic Field Laboratory (GHMFL), in the field range between 12 and 17 T (i.e., 510–723 MHz). The ESR measurements are analyzed in Sec. IV A and the NMR results in Sec. IV B. The conclusions are given in Sec. V.

II. EXPERIMENTAL DETAILS AND DATA ANALYSIS

The hexanuclear spin cluster compound $[\text{Fe}_6(\text{tea})_6] \cdot 6\text{MeOH}$ was synthesized by Geißelmann.¹³ Six iron(III) ions are coordinated and magnetically coupled by the triethanolamine 3- (tea) ligand [Fig. 1(a)].¹³ The molecular symmetry is $\bar{3}$ and the space group $R\bar{3}$ with the lattice parameters $a=23.9866 \text{ \AA}$ and $c=8.9549 \text{ \AA}$. Figure 1(b) shows the arrangement of the iron rings in the crystal structure.

The magnetic properties of the $\text{Fe}_6(\text{tea})_6$ complex have been determined by ESR at 94 GHz (W band) and magnetic susceptibility measurements^{12a,12b} and can be described by the following spin Hamiltonians:

$$\mathcal{H}_{\text{ex}} = -J \sum_{i=1}^6 \vec{s}_i \vec{s}_{i+1}, \quad \vec{s}_1 = \vec{s}_7, \quad (1a)$$

$$\mathcal{H}_{\text{ligand}} = d \sum_{i=1}^6 \left[(s_i^c)^2 - \frac{1}{3} (\vec{s}_i)^2 \right], \quad (1b)$$

$$\mathcal{H}_{\text{dipole}} = (g\mu_B)^2 \frac{1}{2} \sum_{i \neq j}^6 \frac{3}{2} (1 - 3 \cos^2 \Theta_{ij}) \frac{1}{r_{ij}^3} \left(s_i^c s_j^c - \frac{1}{3} \vec{s}_i \vec{s}_j \right), \quad (1c)$$

and

$$\mathcal{H}_{\text{Zeeman}} = g\mu_B \vec{B} \sum_{i=1}^6 \vec{s}_i. \quad (1d)$$

The Hamiltonian $\mathcal{H}_{\text{Fe}_6} = \mathcal{H}_{\text{ex}} + \mathcal{H}_{\text{ligand}} + \mathcal{H}_{\text{dipole}} + \mathcal{H}_{\text{Zeeman}}$ includes the Heisenberg exchange interaction \mathcal{H}_{ex} , the on-site anisotropy of the spin \vec{s}_i , $\mathcal{H}_{\text{ligand}}$, which is caused by the ligand configuration of the iron(III) ion, the intramolecular dipolar interaction $\mathcal{H}_{\text{dipole}}$ (r_{ij} denotes the vector connecting spins i and j , Θ_{ij} is the angle of r_{ij} with respect to the quantization axis c , and μ_B is Bohr's magneton, $r_{i,i+1} = 3.201 \text{ \AA}$, $\Theta_{ij} = 90^\circ$), and the Zeeman interaction $\mathcal{H}_{\text{Zeeman}}$. $\mathcal{H}_{\text{ligand}}$ and $\mathcal{H}_{\text{dipole}}$ are invariant with respect to the $\bar{3}$ symmetry of the molecule and $\mathcal{H}_{\text{Fe}_6}$ transforms like the total sym-

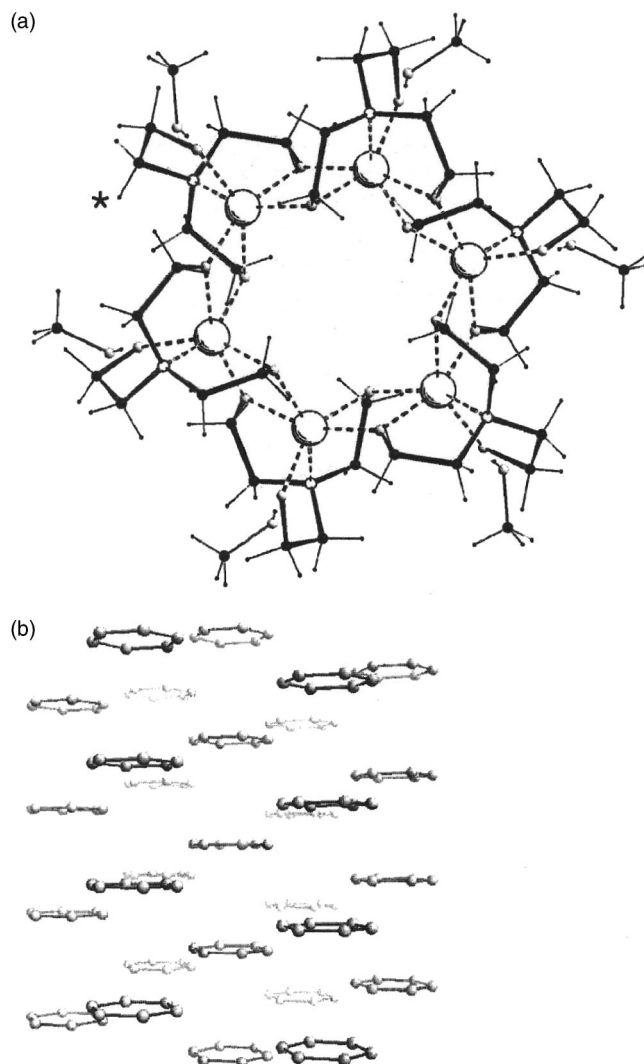


FIG. 1. (a) “SCHAKAL” view of $\text{Fe}_6(\text{tea})_6$ complex and the surrounding six methanol molecules along the $\bar{3}$ symmetry axis (c axis). The large white spheres indicate Fe atoms and the small white, gray, and black dots N, O, and C atoms, respectively. The needles point to the H atoms. The asterisk indicates the H atom, which is used for the calculation of the NMR properties. (b) View of the relative arrangement of the iron rings perpendicular to $\bar{3}$.

metric representation of the point group 6 concerning the cyclic permutations of the indices i . The intramolecular exchange constant $J/k_B = -31.5 \text{ K}$ was determined by measurements of the static magnetic susceptibility and the parameter of $\mathcal{H}_{\text{ligand}}$ $d/k_B = -0.603 \pm 0.008 \text{ K}$ by ESR at 94 GHz.^{12a,12b} $(Ns)^2 d/2J = 2.15$, and the condition for Néel vector tunneling in zero magnetic fields, $(Ns)^2 d/2J > 4$,^{6b,9} is not satisfied. The g factor is nearly independent of the magnetic field direction, $g_{\parallel} = 2.0000$, $g_{\perp} = 1.9955$, and $g = 2$ is used in $\mathcal{H}_{\text{Zeeman}}$ [Eq. (1d)]. The degeneracy of the energy levels of \mathcal{H}_{ex} is lifted by $\mathcal{H}_{\text{ligand}}$, $\mathcal{H}_{\text{dipole}}$, and $\mathcal{H}_{\text{Zeeman}}$ and the spin states of \mathcal{H}_{ex} are mixed due to the influence of $\mathcal{H}_{\text{ligand}}$ and $\mathcal{H}_{\text{dipole}}$. Nevertheless, the magnetic properties of the molecule are still dominated by the isotropic exchange interaction so that the quantum number of the total spin S remains a useful quantity for the characterization of the eigenstates of $\mathcal{H}_{\text{Fe}_6}$.

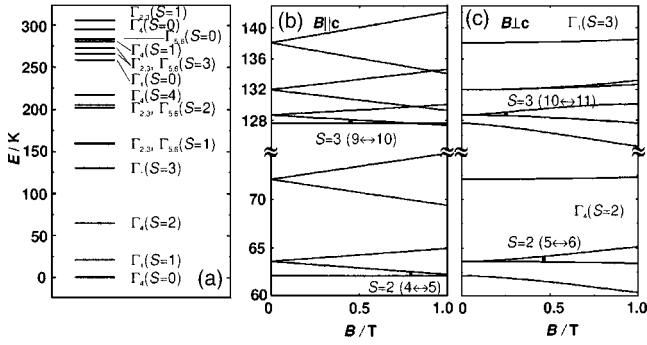


FIG. 2. (a) Low-energy range of the eigenstates of \mathcal{H}_{ex} ; (b) and (c) zero-field and Zeeman splitting of the lowest excited spin states $S=2$ and 3 predicted by Hamiltonian $\mathcal{H}_{\text{Fe}_6}$ [Eq. (1)] for parallel and perpendicular orientation of the magnetic field B , respectively. The parameters of $\mathcal{H}_{\text{Fe}_6}$ are given in the text. The transitions observed by ESR at 9.44 GHz are indicated in (b) and (c) and characterized by the numbers of the corresponding excited energy levels above the ground state.

(Fig. 2). The sixfold symmetry of Hamiltonian $\mathcal{H}_{\text{Fe}_6}$ with respect to cyclic permutations is strictly conserved. This leads to six irreducible representations Γ_t ($t=1,2,\dots,6$) which form orthogonal subsets of eigenstates even when a magnetic field B is applied in any orientation.¹⁴ Figure 2(a) shows the low-energy range of the eigenvalue spectrum of \mathcal{H}_{ex} with the spin and permutation symmetry of the energy levels. The Zeeman effect of the first excited spin states $S=2$ and 3 for parallel and perpendicular field orientations is given in Figs. 2(b) and 2(c), respectively. Figures 2(b) and 2(c) show also the ESR transitions which will be discussed in the following. The level crossing between $\Gamma_4(S=0)$ and the lowest level of $\Gamma_1(S=1)$ for $B \perp c$ was studied by ^1H NMR. The calculation predicts the level crossing at $B_c=15.02$ T. The smallness of the ^1H Larmor frequency (~ 640 MHz at 15 T) makes the NMR technique particularly sensitive to small perturbations which can prevent an exact level crossing as would be expected according to the Hamiltonian Eq. (1). The perturbation has to break the permutation symmetry of $\mathcal{H}_{\text{Fe}_6}$ so that eigenstates of Γ_1 and Γ_4 symmetry are no longer strictly orthogonal. The antisymmetric Dzyaloshinski-Moriya¹⁵ interaction reduces the permutation symmetry of $\mathcal{H}_{\text{Fe}_6}$ whereas the symmetric pseudodipolar exchange interaction¹⁵ behaves similarly to the dipolar interaction and does not reduce the permutation symmetry of $\mathcal{H}_{\text{Fe}_6}$. The Dzyaloshinski-Moriya interaction

$$\mathcal{H}_{\text{DM}} = \sum_{i=1}^6 \vec{D}(-1)^i (\vec{s}_i \times \vec{s}_{i+1}) \quad (1e)$$

is compatible with the molecular symmetry $\bar{3}$. The vector \vec{D} is parallel to the molecular symmetry axis. \mathcal{H}_{DM} transforms with respect to cyclic permutations of the indices i like Γ_4 and induces in first-order perturbation no splitting of the $\Gamma_t(S)$ states. Therefore, its influence cannot be easily detected in standard ESR experiments. \mathcal{H}_{DM} reduces the cyclic permutation symmetry from 6 to 3, the states of symmetry Γ_1 and Γ_4 are no longer orthogonal, and a level anticrossing can

be expected. The influence of \mathcal{H}_{DM} will be discussed in Sec. IV B.

The small angular dependence of the g factor indicates that the g tensors of the individual iron ions cannot be simply replaced by a single g value. Deviations of the local g factors at the sites of the iron(III) from the mean g factor will also reduce the permutation symmetry but, as will be shown in the following, do not lead to a mixing of Γ_1 and Γ_4 eigenstates. The general form of the Zeeman Hamiltonian is $\mathcal{H}_{\text{Zeeman}} = \mu_B \sum_{i=1}^6 \sum_{\mu,\mu'} g_{\mu,\mu'}^i s_{\mu,\mu'}^i B^{\mu,\mu'}$, denotes the g tensor of the iron ion i . Although the principal g values of the tensor $g_{\mu,\mu'}^i$ are the same for each ion, the principal axes of the tensors are different, so that the matrices $g_{\mu,\mu'}^i$ in the reference frame of the $\text{Fe}_6(\text{tea})_6$ molecule are in general not identical. The application of the $\bar{3}$ symmetry transformation leads to the equation $g_{\mu,\mu'}^i = g_{\mu,\mu'}^{i+3}$, which shows that only the Zeeman energies of the ion pairs $i, i+3$ are equal, when a magnetic field $B \parallel c$ is applied. The cyclic permutation symmetry is thus reduced from 6 to 2, but the eigenstates of symmetry Γ_1 and Γ_4 remain orthogonal, so that the Zeeman interaction cannot induce a level anticrossing of Γ_1 and Γ_4 states.

In the following (and in the Appendix) we give an overview of ESR and NMR data analysis as used in the present work. The ESR experiment measures the microwave absorption which is given by the imaginary part of the dynamic susceptibility¹⁶

$$\chi''_{xx}(\nu) = \frac{1}{2\hbar V} \left[1 - \exp\left(-\frac{\hbar\nu}{k_B T}\right) \right] \int_{-\infty}^{\infty} \langle M_x(\tau) M_x(0) \rangle \times \exp(+i2\pi\nu\tau) d\tau. \quad (2)$$

V is the volume of the sample, the microwave field B_1 oscillates along the x direction (the static field B is applied along z), and \vec{M} denotes the total magnetic moment $\vec{M} = g\mu_B \sum_{j=1}^N \vec{S}^{(j)}$ of a sample that contains N iron rings. $\vec{S}^{(j)} = \sum_{i=1}^6 \vec{s}_i^{(j)}$ is the total spin of ring j , and $\vec{s}_i^{(j)}$ the spin of an individual iron(III) ion.

The longitudinal relaxation of the nuclear ^1H spin demands more comments. It is assumed throughout the following discussion that only the coupling of the ^1H nuclear spin to the iron ring to which it is attached contributes to the relaxation. The protons are coupled to the iron(III) ions of the ring by the dipolar interaction $\mathcal{H}_1^{\text{dipolar}} = \sum_{i=1}^6 \hbar^2 (\gamma_s \gamma_I / r_i^3) \times [\vec{s}_i \vec{I} - 3(\vec{s}_i \vec{r}_i)(\vec{I} \vec{r}_i) / r_i^2]$ and the transferred hyperfine interaction $\mathcal{H}_1^{\text{hf}} = \hbar \sum_{i=1}^6 A_i \vec{s}_i \vec{I}$ which can both be written as $\mathcal{H}_1 = \hbar(F^z I^z + F^+ I^- + F^- I^+)$ with

$$F^z = \sum_{i=1}^6 \left[\frac{2}{3} D_0(i) s_i^z + D_{+1}(i) s_i^+ + D_{-1}(i) s_i^- \right],$$

$$F^{\pm} = \sum_{i=1}^6 \left[-\frac{1}{6} D_0(i) s_i^{\mp} + D_{\pm 1}(i) s_i^z + D_{\pm 2}(i) s_i^{\pm} \right] \quad (3a)$$

for the dipolar coupling and

$$F^z = \sum_{i=1}^6 A(i) s_i^z,$$

$$F^\mp = \sum_{i=1}^6 \frac{1}{2} A(i) s_i^\pm \quad (3b)$$

for the scalar hyperfine interaction. The geometrical factors of the dipolar coupling are $D_0(i) = \alpha_i(3 \cos^2 \Theta_i - 1)$, $D_{\pm 1}(i) = \alpha_i \sin \Theta_i \cos \Theta_i \exp(\mp i \varphi_i)$, $D_{\pm 2}(i) = \frac{1}{2} \alpha_i \sin^2 \Theta_i \exp(\mp 2i \varphi_i)$, with $\alpha_i = 3 \gamma_I \gamma_S \hbar / 2 r_i^3$.¹⁷ $\gamma_I / 2\pi = 42.52$ MHz/T denotes the gyromagnetic ratio of the ¹H nucleus and $\gamma_S / 2\pi = g \mu_B / \hbar = 27.99$ GHz/T with $g=2$. The z direction is determined by the direction of the magnetic field and the angles Θ_i and φ_i specify the orientation of the vector \vec{r}_i with respect to \vec{B} . The longitudinal relaxation for a spin- $\frac{1}{2}$ nucleus was calculated by Moriya:¹⁸

$$\frac{1}{T_1} = \int_{-\infty}^{+\infty} \langle F^-(\tau) F^+(0) \rangle \exp(-i 2\pi \nu_0 \tau) d\tau$$

$$+ \int_{-\infty}^{+\infty} \langle F^+(\tau) F^-(0) \rangle \exp(+i 2\pi \nu_0 \tau) d\tau$$

$$= [1 + \exp(-h \nu_0 / k_B T)] \int_{-\infty}^{+\infty} \langle F^+(\tau) F^-(0) \rangle$$

$$\times \exp(+i 2\pi \nu_0 \tau) d\tau. \quad (4)$$

$2\pi \nu_0 = \gamma_I B$ denotes the ¹H Larmor frequency. The shift of the Larmor frequency due to the local magnetic field is small (compare Fig. 8) and can be neglected, since the fluctuation spectrum $\int_{-\infty}^{+\infty} \langle F^+(\tau) F^-(0) \rangle \exp(+i 2\pi \nu \tau) d\tau$ extends over a large frequency range (≥ 200 MHz; see below and Figs. 10–12). The nuclear relaxation is caused by the fluctuation of the spin $\vec{s}_i(\tau)$ of the iron(III) ions. The thermal oscillation of protons in the solid state cannot contribute to the nuclear relaxation since the corresponding frequencies are too high (100 GHz or larger). Most of the transition frequencies between the eigenstates of the iron ring are as well very much larger than ν_0 , so that only the operator $D_{\pm 1}(i) s_i^\pm$ of the dipolar coupling can contribute to T_1^{-1} efficiently, since it also allows for NMR transitions involving only one electronic state. The operators s_i^\pm are effective when the separation between two energy levels is comparable with the nuclear Zeeman splitting. Then both the dipolar coupling and the transferred hyperfine interaction can contribute to the nuclear relaxation.

The description of the microwave absorption and the nuclear relaxation leads to spectral densities of the general form $f(\nu) = \int_{-\infty}^{+\infty} \langle A(\tau) B(0) \rangle \exp(+i 2\pi \nu \tau) d\tau$. The operators $A = \sum_{j=1}^N A^{(j)}$ and $B = \sum_{j=1}^N B^{(j)}$ denote either the magnetic moment of the sample $A = B = M_x = g \mu_B \sum_{j=1}^N S_x^{(j)}$ (microwave absorption), or the operators F^\pm for the longitudinal nuclear relaxation (in this case the sum is reduced to one term $N=1$). The dynamics of the iron spin $\vec{s}_i(\tau)$ is dominated by the Hamiltonian $\mathcal{H}_{\text{Fe}_6}$ of the iron rings. In the case when all iron rings within the sample are identical and independent from each other, it is possible to calculate the spectral density $f(\nu)$ in

terms of the eigenvalues and eigenstates of one ring j , $\mathcal{H}_{\text{Fe}_6}^{(j)} |\mu\rangle = E_\mu^{(j)} |\mu\rangle$, and $f(\nu)$ becomes

$$f(\nu) = \frac{2\pi}{Z} \sum_{\mu, \mu'} \exp(-E_\mu^{(j)} / k_B T) \langle \mu | A^{(j)} | \mu' \rangle$$

$$\times \langle \mu' | B^{(j)} | \mu \rangle \delta \left(\frac{(E_\mu^{(j)} - E_{\mu'}^{(j)})}{h} + \nu \right) \quad (5)$$

with $Z = \sum_\mu \exp(-E_\mu^{(j)} / k_B T)$. The spectrum of $f(\nu)$ consists of δ -shaped resonances at $\nu=0$ and $\nu_{\mu, \mu'} = (E_\mu - E_{\mu'}) / h$, due to transitions between the eigenstates of $\mathcal{H}_{\text{Fe}_6}^{(j)}$. The intensity of the resonances is determined by the eigenstates of $\mathcal{H}_{\text{Fe}_6}^{(j)}$ and the operators $\vec{S}^{(j)} = \sum_{i=1}^6 \vec{s}_i^{(j)}$ and F^\pm , respectively. The total spin $\vec{S}^{(j)} = \sum_{i=1}^6 \vec{s}_i^{(j)}$ is important for the description of the ESR experiments and transforms according to Γ_1 , so that only transitions between states with the same permutation symmetry can be observed. In the case of NMR experiments the operators F^\pm are formed by the individual spins \vec{s}_i of the iron ions. These spin operators can be decomposed into the irreducible components of the permutation group. The even component of \vec{s}_i , which is proportional to the total spin $\vec{s}_{\Gamma_1} \propto \sum_{i=1}^6 \vec{s}_i^{(j)}$, dominates in most cases the nuclear relaxation, since the condition $\nu_{\mu, \mu'} = (E_\mu - E_{\mu'}) / h = \nu_0 \approx 0$ can be usually realized only by eigenstates of the same symmetry. Only in the case of the level crossing do other components of \vec{s}_i become important. In the case when the energies of the lowest $\Gamma_4(S=1)$ and the $\Gamma_1(S=0)$ levels become nearly equal, the odd component of \vec{s}_i , which is proportional to $\vec{s}_{\Gamma_4} \propto \sum_{i=1}^6 (-1)^i \vec{s}_i$, can contribute to relaxation. Under these conditions the NMR experiment becomes sensitive to the dynamics of the Néel vector n . Since the selection rules of the total spin $\vec{S}^{(j)} = \sum_{i=1}^6 \vec{s}_i^{(j)}$ and the operators F^\pm introduce differences between the spectral density of the ESR and NMR experiments we use in the following the notation $f_{\text{ESR}}(\nu)$ and $f_{\text{NMR}}(\nu)$, respectively.

The perturbation of $\mathcal{H}_{\text{Fe}_6}^{(j)}$ by spin-phonon interaction or by an intermolecular spin-spin interaction is the reason that the δ functions in Eq. (5) have to be replaced by normalized shape functions which have a finite width. The shape and width of the resonances of $f_{\text{ESR}}(\nu)$ can be directly observed by the ESR lines in the case of the microwave absorption [Eq. (2)], whereas the shape and width of the resonances of $f_{\text{NMR}}(\nu)$ enter into the description of the nuclear relaxation via Eq. (4). The understanding of the intensity, shape, and width of the resonances of $f_{\text{ESR}}(\nu)$ and $f_{\text{NMR}}(\nu)$ is therefore particularly important for the discussion of the ESR and NMR results.

Since the intermolecular dipolar interaction is determined by the crystal structure it is convenient to calculate its influence on the spectral density by the so-called method of moments.¹⁹ The first three moments determine the intensity $m_0 = \int_{\text{around } \nu_0} f(\nu) d\nu$, the shift of the resonance frequency due to the perturbation $m_1 = (1/m_0) \int (\nu - \nu_0) f(\nu) d\nu$, and the width of the resonance $m_2 = (1/m_0) \int (\nu - \nu_0)^2 f(\nu) d\nu$ at $\nu_0 = (E_\mu - E_{\mu'}) / h$. The spectral density around the transition fre-

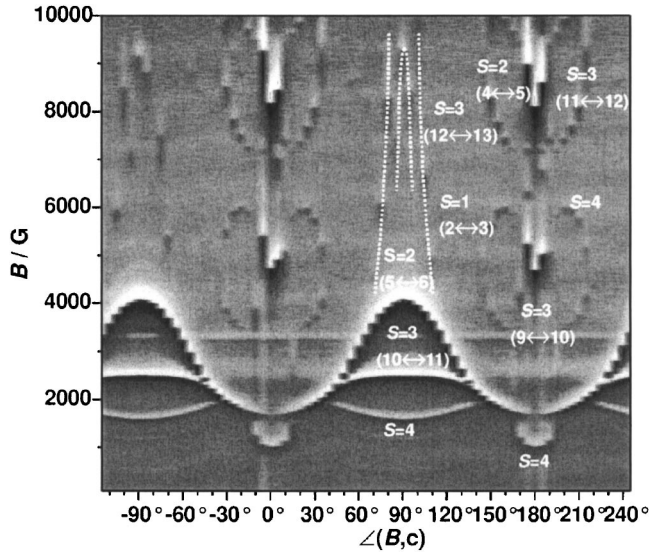


FIG. 3. Contour plot of the angular variation of the ESR spectra at $\nu=9.44$ GHz measured in steps of 5° for $T=30$ K [black (white) indicates positive (negative) signal intensity]. The resonances are assigned by means of Hamiltonian $\mathcal{H}_{\text{Fe}_6}$ [Eq. (1)] and the parameters given in the text. The dashed lines are guides for the eye. The resonances which do not shift with the orientation of B originate from impurities within the resonator.

quency ν_0 can be approximated by Gaussian lines $f(\nu)|_{\nu \approx \nu_0} = (m_0/\sqrt{2\pi m_2})\exp\{-[(\nu-\nu_0)+m_1]^2/2m_2\}$. Higher moments are necessary for the complete characterization of the resonance lines. Explicit formulas for the calculation of the first three moments in terms of the eigenvalues $E_\mu^{(j)}$ and eigenfunctions $|\mu\rangle$ of the unperturbed Hamiltonian are reported by McMillan and Opechowski²⁰ and Zevin and Shanina.²¹ Their formulas will be used in the following. Details about the method of moments and the intermolecular dipolar interaction are given in the Appendix.

When the perturbation \mathcal{H}' becomes time dependent due to motion, the Gaussian line shape transforms into a Lorentzian. The linewidth is narrowed according to $\Delta\nu \approx m_2\tau_c$, when the correlation time τ_c is short $\sqrt{m_2} < (1/\tau_c)$.²² The parameter τ_c will not be used in the following.

III. RESULTS

A. ESR results

The ESR spectra of $\text{Fe}_6(\text{tea})_6$ crystals were measured with an ESP300E Bruker spectrometer ($\nu=9.44$ GHz), equipped with an Oxford Instrument cryostat. In contrast to our previous work which focused on the position of the ESR resonances in order to determine the parameters of the Hamiltonian $\mathcal{H}_{\text{Fe}_6}$,¹² we discuss in this paper the spin dynamics and analyze the angular variation and temperature dependence of the ESR linewidth. The contour plot (Fig. 3) gives an overview of the angular variation $\sphericalangle(B,c)$ of the spectra at $T=30$ K. The first derivative of the absorption spectra are measured in steps of 5° . The oscillating microwave field B_1 was oriented perpendicular to c for all experiments. The

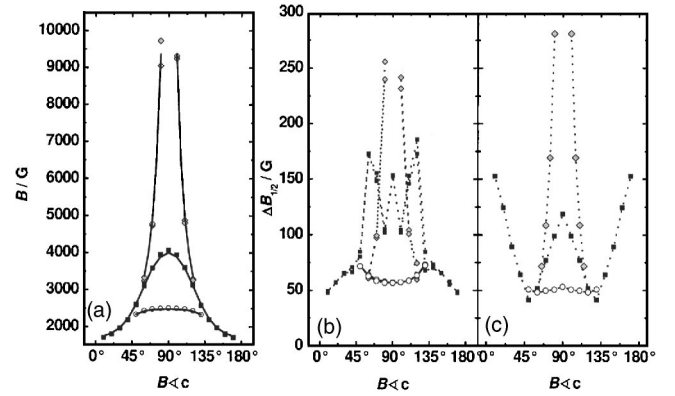


FIG. 4. Angular dependence of the ESR lines measured for $T=25$ K. Transition $S=1$ ($2 \leftrightarrow 3$), gray diamonds; $S=2$ ($5 \leftrightarrow 6$), black squares; and $S=3$ ($10 \leftrightarrow 11$), circles. (a) Resonance field strength of the ESR lines. The solid lines are calculated with Hamiltonian $\mathcal{H}_{\text{Fe}_6}$ [Eq. (1)]. (b) Experimentally determined linewidth and (c) calculation of the linewidth (see Sec. IV A). The dotted lines are guides for the eye.

resonances can be assigned to transitions within the first excited states $S=1, 2, 3,$ and 4 by means of the Hamiltonian $\mathcal{H}_{\text{Fe}_6}$.

It is interesting to note that in the energy range between the $S=3$ and 4 states there are four additional $S=1$ and 2 states ($\Gamma_{2,3}, \Gamma_{5,6}$) for which no ESR signals could be detected, which could be due to fast spin-lattice relaxation (see below). Figure 4 shows the angular dependence of the ESR resonance fields and linewidth which are assigned to the transitions $S=1$ ($2 \leftrightarrow 3$), 2 ($5 \leftrightarrow 6$), and 3 ($10 \leftrightarrow 11$) (compare Fig. 2). The angular shift of the resonance fields can be calculated by Hamiltonian $\mathcal{H}_{\text{Fe}_6}$ and enables the assignment of the ESR lines [solid lines in Fig. 4(a)]. The angular dependence [Fig. 4(b)] and the temperature dependence of the ESR linewidth of the transitions within the $S=2$ and 3 states for parallel and perpendicular field orientation (Fig. 5) will be discussed in Sec. IV A.

B. NMR results

For proton NMR at $\nu_0=52$ MHz a Bruker CXP 200 spectrometer and an electromagnet were used with an Oxford Instruments variable-temperature cryostat. Measurements between 12 and 17 T were performed at the GHMFL with a home-built pulsed NMR spectrometer in a 17 T variable-field superconducting magnet, within the standard variable-temperature cryostat and in a dilution refrigerator. The crystal orientation was $B \perp c$ during all experiments. The spin-lattice relaxation time T_1 was determined by an inversion-recovery spin-echo sequence with phase cycling ($\pi/2$ pulse length was $1.5 \mu\text{s}$). The long relaxation times (≥ 1 s) at 200 mK [see Fig. 7(a)] were determined by a saturation recovery spin-echo sequence. The relaxation of the magnetization at $\nu_0=52$ MHz ($B=1.22$ T) is monoexponential at all temperatures [Fig. 6(a)] and the T_1^{-1} rate follows the expected temperature dependence^{4(a)} which is characterized by a peak at ≈ 40 K and a linear increase for $T \geq 100$ K [Fig. 6(b)].

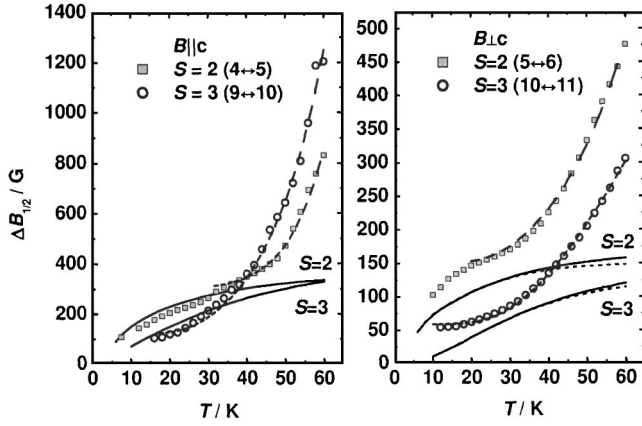


FIG. 5. Temperature dependence of the ESR linewidth for parallel and perpendicular field orientation. The experimental results (dots) are compared with the expected temperature dependence due to the spin-lattice relaxation which is approximated by Eq. (7) (dashed lines) and the contribution of dipolar intercluster interaction (solid lines). The thick solid lines are obtained when the lowest spin states $S=0, 1, 2$, and 3 are included into the calculation. The dotted lines result when all the spin states up to $\Gamma_4(S=4)$ are included [see Fig. 2(a)], and reveal slight modifications only for $B \perp c$. The parameters are given in Table I (the constant offset ΔB_0 for $S=2$ below $T \lesssim 30$ K is not plotted). The details are explained in Sec. IV A.

The T_1^{-1} rate in the field range between 12 and 17 T [Fig. 7(a)] has a peak due to a resonance between the nuclear spins and the electronic spin dynamics of the iron(III) ring, which is caused by the crossing of the ground state and the first excited energy level.^{23,24} The enhanced T_1^{-1} rate around 15 T can be described by a phenomenological approach as was proposed by Affronte *et al.*²⁵ However, in contrast to the previously reported results for Fe_6 and Fe_{10} compounds,^{23–25} the peak has a Gaussian instead of a Lorentzian shape and can be approximated by the formula $T_1^{-1} \propto \exp[-(\hbar \gamma_I B - \Delta)^2 / 2\Gamma^2]$. $\Delta = g\mu_B |B_c - B|$ denotes the energy gap in the

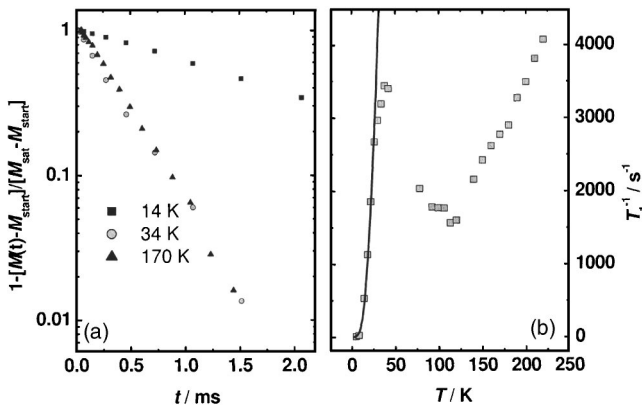


FIG. 6. (a) Relaxation of the magnetization. M_{start} denotes magnetization which can be inverted and M_{sat} the totally relaxed equilibrium magnetization. (b) Temperature dependence of the ^1H T_1^{-1} rate (squares), $B=1.2$ T. The solid line shows the result of a calculation (the calculation is scaled at $T=30$ K to the experimental value; for details see Sec. IV B).

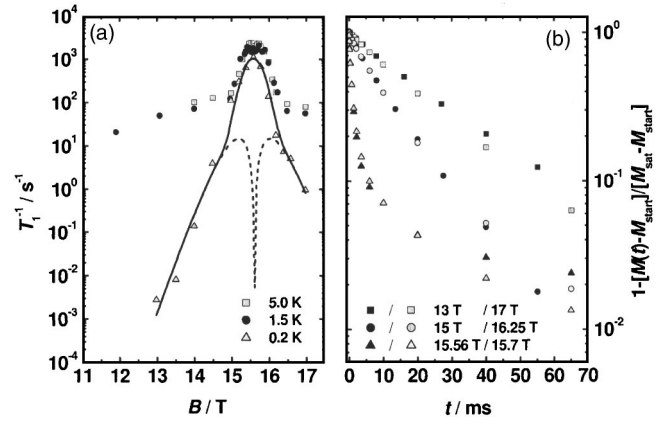


FIG. 7. (a) T_1^{-1} rate measured for $B \perp c$ in the field range of the first level crossing (compare Fig. 2). The solid line shows the phenomenological description of the T_1^{-1} rate due to spin-spin and spin-phonon relaxation as discussed in Sec. III B. The dashed lines show the expected T_1^{-1} rate due to spin-phonon relaxation only. (b) Relaxation of the magnetization for $T=1.5$ K.

crossing region. The parameters are $B_c = 15.61 \pm 0.03$ T and $\Gamma = 0.20 \pm 0.02$ T. The half-width of the T_1^{-1} peak ($\Delta B_{1/2} = \sqrt{2 \ln 2} \Gamma = 0.235$ T) is comparable to the values observed for the Fe_6 [0.26 T (Ref. 25)] and the Fe_{10} [1.04 T (Ref. 24)] compounds, and attributed to a temperature-dependent level broadening.^{24,25} The Gaussian shape of the peak results from an intrinsic inhomogeneity of the $\text{Fe}_6(\text{tea})_6$ system which is discussed in Sec. IV B.

The measurements of the T_1^{-1} rate at $T=200$ mK are important for the discussion of inelastic processes, which could be particularly important, in the vicinity of the level crossing. The measurements at 200 mK reveal that the nuclear relaxation in the magnetic field range below and above the peak is dominated by a two-phonon process, in which the phonons bridge the gap between the ground state and the first excited state of the iron(III) ring. According to Orbach the T_1^{-1} rate is given by $T_1^{-1} \propto (\Delta/g\mu_B)^3 / [\exp(\Delta/k_B T) - 1]$,²⁶ where Δ denotes the energy gap as before. The solid line in Fig. 7(a) shows the combined contributions due to the spin-phonon relaxation and the resonance between the nuclear and electronic spin systems according to $T_1^{-1} = a(\Delta/g\mu_B)^3 / [\exp(\Delta/k_B T) - 1] + b \exp[-(\hbar \gamma_I B - \Delta)^2 / 2\Gamma^2]$ with $a = 3170 \text{ s}^{-1} \text{ T}^{-3}$ and $b = 1050 \text{ s}^{-1}$, while the dashed line shows only the contribution of the spin-phonon relaxation. The exponential increase of the T_1^{-1} rate is efficiently stopped and reversed in the vicinity of the level crossing due to the temperature-independent factor $(\Delta/g\mu_B)^3$, which accounts for the phase space of the phonons. It can be therefore expected that spin-phonon processes will not considerably interfere with spin-spin processes in the range of the level crossing, although excitations to higher-lying states might actually prevent the spin-phonon relaxation from going to zero at the level crossing.

The relaxation of the magnetization as a function of time is shown in Fig. 7(b) for some selected field values at $T=1.5$ K. The relaxation outside the crossing region is monoexponential. The relaxation of the magnetization in the field range around the peak starts with a fast decay at short

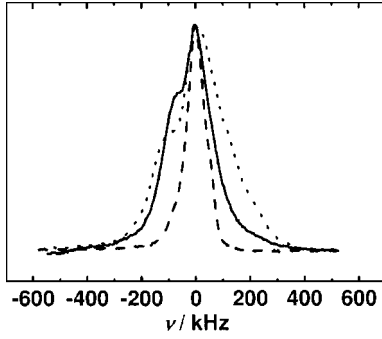


FIG. 8. Comparison between the ^1H NMR spectra measured at $T=1.5$ K and $\nu_0=506.8$ MHz (dashed line, $B=11.9$ T), 663.88 MHz (solid line, $B=15.59$ T), and 722.83 MHz (dotted line, $B=16.98$ T). The spectra are normalized and the peak is adjusted to $\nu=0$.

times and changes into a slow decay for $t \geq 6$ ms. The T_1^{-1} rate in Fig. 7(a) denotes the slope of the relaxation curve for $t \rightarrow 0$.

The spin-spin relaxation time T_2 was determined by a two-pulse spin-echo sequence with phase cycling (pulse length 1.5 μs). For $\nu_0=52$ MHz, the T_2^{-1} rate increases from 33 kHz at $T=5$ K up to 50 kHz at $T \sim 50$ K and becomes nearly temperature independent at higher temperatures. For high frequencies and $T=1.5$ K, the T_2^{-1} rate is 32 kHz at 13 T and 24.7 kHz at 17 T. The ^1H NMR spectra were obtained by the Fourier transform of the free induction decay or of the solid echo (for broad lines). Figure 8 shows ^1H spectra measured at 1.5 K and $B=11.6, 15.6, 17$ T for perpendicular field orientation $B \perp c$. The full width of the spectrum at half height increases from 83 kHz at $B=11.6$ T ($\nu_0=506.8$ MHz) to 186 kHz in the magnetic field range of the level crossing $B_c=15.6$ T ($\nu_0=663.88$ MHz) up to 251 kHz at the highest measured magnetic field strength of $B=17$ T ($\nu_0=722.83$ MHz). The spectrum above the level crossing is clearly split up, which is due to the presence of inequivalent sets of protons, and the transition from a diamagnetic to a paramagnetic system.

The inhomogeneous ^1H NMR spectrum is caused by the strong dipolar interaction between the nuclear spins of the neighboring protons at the carbon sites (compare Fig. 1) and the dipolar interaction between the nuclear spins and the magnetic moments of the iron(III) ions. The energy of a nuclear spin I can be calculated by the approximate Hamiltonian¹⁷

$$\begin{aligned} \mathcal{H}_I = & \hbar \gamma_I B F^z + (\hbar \gamma_I)^2 \sum_{I'} \frac{3}{2} (1 - 3 \cos^2 \Theta_{I,I'}) \left(\frac{1}{r_{I,I'}} \right)^3 \\ & \times \left(F F' - \frac{1}{3} \vec{I} \cdot \vec{I}' \right) + \sum_{i=1}^6 \left[\hbar^2 \gamma_I \gamma_S (1 - 3 \cos^2 \Theta_{I,S_i}) \left(\frac{1}{r_{I,S_i}} \right)^3 \right. \\ & \left. + \hbar A_i \right] F^z \langle s_i^z \rangle. \end{aligned} \quad (6)$$

The first term is the nuclear Zeeman energy, which dominates and determines essentially the resonance frequency.

The second term accounts for the dipolar coupling between the nuclear spins I and I' . The nuclear dipolar coupling is independent of the strength of the applied magnetic field.²⁷ $\Theta_{I,I'}$ denotes the angle between the vector $\vec{r}_{I,I'}$ and the external magnetic field, which is oriented along z . The third term accounts for the dipolar and the hyperfine transferred interaction between the nuclear spin I and the spin of the iron(III) ions. It contains the static expectation value $\langle s_i^z \rangle = (1/6) \times (\chi\text{H}/g\mu_B)$ which makes the ^1H NMR spectrum dependent on the magnetic field strength. Θ_{I,S_i} denotes the angle between the vector \vec{r}_{I,S_i} and the external magnetic field.

The inhomogeneous ^1H NMR spectrum can be simulated by calculating the resonance frequencies of all ^1H nuclear spins according to Eq. (6). Each resonance can be approximated by a Lorentzian line with the width $\Delta\nu_{1/2} = (2\pi T_2)^{-1}$ (half width at half height). The susceptibility of the iron ring is nearly zero at $T=1.5$ K, $B=11.6$ T and it can be expected that the ^1H resonances are only shifted due to the dipolar proton-proton interaction. The simulation predicts for $B \perp c$ a proton spectrum over a frequency range of 86 kHz. The measured ^1H spectra reveal no fine structure and an intrinsic linewidth of the proton resonance of $\Delta\nu_{1/2} \sim 30$ kHz has to be chosen in order to simulate the experimental results. This is more than what is expected from the experimentally determined T_2^{-1} rate, and points to some inhomogeneous line broadening. The dipolar coupling between the magnetic moments of the iron(III) ions and the protons becomes important, when the average magnetic moment of the iron ring is not negligible small. The magnetic moment of the iron ring increases steplike in the magnetic field range of the level crossing and the ^1H spectra starts to broaden with increasing field strength. A simulation of the spectra based on the 72 protons of the $\text{Fe}_6(\text{tea})_6$ ring predicts that the spectra of 48 protons are shifted up to higher frequencies whereas the spectra of 16 protons are almost not shifted. A small group of eight protons is expected to be shifted strongly to smaller frequencies. The shoulder in the left wing of the ^1H spectrum at $T=1.5$ K and $B=15.59, 17$ T confirms the results of these simulations.

IV. DISCUSSION

A. ESR measurements

The contour plot in Fig. 9 illustrates $\chi''_{xx}(\nu, B)$ for $B \perp c$, $x \perp c$, and $T=15$ K as a function of the magnetic field B and the frequency ν . The calculation of $\chi''_{xx}(\nu, B)$ includes the moments m_0 and m_2 . The position of the resonances is determined by the intramolecular Hamiltonian $\mathcal{H}_{\text{Fe}_6}$ and the shift of the resonances due to the intermolecular dipolar interaction which is determined by the first moment m_1 is small and can be neglected. The region in the (ν, B) space, which can be tested with the experimental parameters $\nu=9.44$ GHz and $0 < B < 1$ T, is indicated by a solid line. In agreement with the experimental results, Fig. 9 shows that the intensity and the linewidth of the resonances become smaller when the excitation energy of the involved spin states becomes larger. It is possible to calculate the field strength, the linewidth, the

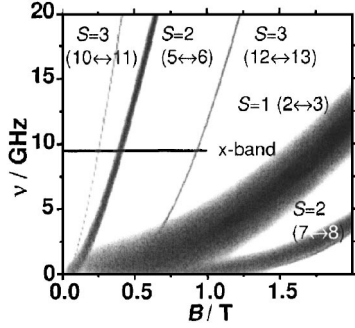


FIG. 9. Contour plot of $\chi''_{xx}(\nu, B)$ calculated for $B \perp c$, $x \perp c$, and $T = 15$ K (black, high values of χ''_{xx} ; white, $\chi''_{xx} = 0$). The range that is experimentally accessible with the x -band Bruker spectrometer is indicated by the black line. The resonance lines are denoted by the spin S and the numbers of the excited energy levels that are involved in the transition.

angular variation ($\angle B, c$), and the temperature dependence of the resonances.

The quantitative comparison between the experimental results and the numerical predictions is shown in Figs. 4 and 5. The angular variation of the line position measured at $T = 25$ K for the transitions $S=1$ ($2 \leftrightarrow 3$), 2 ($5 \leftrightarrow 6$), and 3 ($10 \leftrightarrow 11$) can be reproduced by the calculation [Fig. 4(a)]. This confirms that $\mathcal{H}_{\text{Fe}_6}$ correctly describes the energy levels and spin states of the $\text{Fe}_6(\text{tea})_6$ ring. Figure 4(b) shows the experimentally determined angular dependence of the linewidth of the transitions $S=1$ ($2 \leftrightarrow 3$), 2 ($5 \leftrightarrow 6$), and 3 ($10 \leftrightarrow 11$) measured at $T = 25$ K and Fig. 4(c) the linewidth predicted by the calculation of the second moment due to the intermolecular dipolar interaction. $\Delta B_{1/2}$ denotes the half width at half height of the absorption line independently of the shape of the absorption line. The measured resonances have Lorentzian line shapes whereas the calculation of the second moment m_2 can only describe Gaussian lines. The Lorentzian line shape indicates the presence of fluctuations which might be caused by small intermolecular exchange interaction. The angular dependence and even the size of the linewidth is well reproduced for transitions between the energy levels of the $S=1$ and 3 eigenstates. Characteristic differences are found for the $S=2$ transition. The peaks of $\Delta B_{1/2}$ for $\angle(B, c) = 60^\circ, 120^\circ$ cannot be reproduced by the calculation. This indicates that not only the intermolecular dipolar interaction but also additional interactions contribute to the perturbation of $\mathcal{H}_{\text{Fe}_6}$.

The temperature dependence of $\Delta B_{1/2}$ is another important source of information. The solid lines in Fig. 5 show the expected temperature variation due the dipolar intercluster interaction, when the lowest spin states $S=0, 1, 2$, and 3 are included into the calculation. The dotted lines show the temperature variation, when all spin states up to the first excited $S=4$ states are included [see Fig. 2(a)]. For $B \parallel c$ the modification of $\Delta B_{1/2}$ is so small that the differences between the two calculations cannot be resolved in Fig. 5. For $B \perp c$ there is only a small reduction of $\Delta B_{1/2}$ for $T \gtrsim 30$ K, when the excited spin states are included into the calculation. There is obviously no crucial influence of excited spin states on the linewidth of the first excited $S=2$ and 3 spin states. The

TABLE I. The parameters of the spin-lattice relaxation [Eq. (7)].

Transition	ΔB_0 G	a (G/K^7)	b (G)	ΔE (K)
$S=2$ ($4 \leftrightarrow 5$)	300	1.8×10^{-10}	436	131
$S=3$ ($9 \leftrightarrow 10$)	120	1.8×10^{-10}	4850	131
$S=2$ ($5 \leftrightarrow 6$)	150	3.3×10^{-11}	1924	131
$S=3$ ($10 \leftrightarrow 11$)	59	—	1915	131

saturation behavior predicted by the calculation is experimentally confirmed by the $S=2$ transitions below ≈ 35 K. The linewidth increases strongly toward higher temperatures and indicates the onset of spin-lattice relaxation. Evidence that spin-lattice relaxation is important is given by the temperature dependence of the $S=3$ transitions, which do not follow the calculated temperature dependence at all. A phenomenological description of $\Delta B_{1/2}$ is possible in terms of the Raman and Orbach processes.²⁶ The dashed lines in Fig. 5 are calculated by the following formula:

$$\Delta B_{1/2} = \Delta B_0 + aT^7 + \frac{b}{[\exp(\Delta E/k_B T) - 1]}. \quad (7)$$

ΔB_0 denotes the linewidth which is not caused by spin-lattice relaxation. The parameters ΔB_0 , a , b , and ΔE are given in Table I. ΔB_0 is for $S=2$ and $T \lesssim 30$ K not constant but temperature dependent as was discussed above. The description by Eq. (7) is not unique and may be considered as a parametrization of the experimental results. Therefore errors are not given. It is, however, interesting to note that the linewidth of the transition $S=3$ ($10 \leftrightarrow 11$) is clearly determined by an Orbach process with an activation energy of $\Delta E/k_B \approx 131$ K, which corresponds well to the excitation energy of the $S=3$ energy levels (compare Fig. 2). ΔE is kept constant for all the other transitions in order to reduce the arbitrariness. The somewhat steeper slope of the $S=2$ ($5 \leftrightarrow 6$) transition leads to a small contribution of the Raman term. The Raman contribution dominates the high-temperature linewidth of the transition $S=2$ ($4 \leftrightarrow 5$) whereas the transition $S=3$ ($9 \leftrightarrow 10$) needs both terms.

The analysis of the ESR results leads to the following conclusions. The temperature range can be divided into a high-temperature range above ≈ 35 K, which is dominated by spin-lattice relaxation, and a low-temperature range, which is determined by the Hamiltonian of the iron ring $\mathcal{H}_{\text{Fe}_6}$ and fluctuating perturbations inducing the experimentally observed Lorentzian line shapes. In particular, the $\Delta B_{1/2}$ angular dependence of the transition $S=2$ ($5 \leftrightarrow 6$) shows that the intermolecular dipolar coupling is not the only contributing perturbation. The phenomenological description of the spin-lattice relaxation shows that each transition is specifically influenced by phonons. This observation might explain the experimental result that the transition of the $\Gamma_{2,3}$ and $\Gamma_{5,6}$ $S=1$ and 2 energy levels cannot be observed by ESR measurements although they are energetically in between the Γ_4 ($S=3$) and Γ_4 ($S=4$) levels, which are observed by ESR [com-

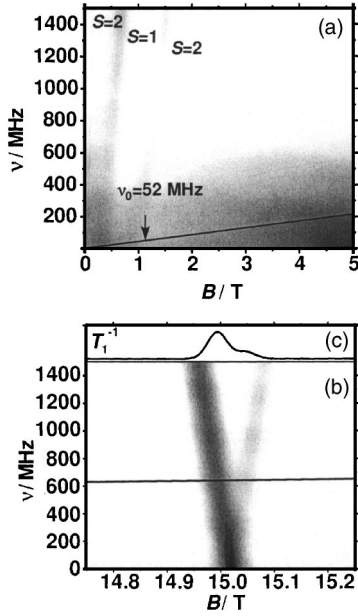


FIG. 10. Contour plot of $T_1^{-1}(\nu, B)$ calculated for (a) $B \perp c$, $T = 15$ K, and $B < 5$ T, and (b) $B \perp c$, $T = 3$ K, in the field range of the first level crossing (black, high values of T_1^{-1} ; white, $T_1^{-1} = 0$). The variation of the ^1H Larmor frequency $\nu_0 = \gamma_H B / 2\pi$ is indicated by a solid line. (c) T_1^{-1} (arb. units) for $\nu_0 = \gamma_H B / 2\pi$.

pare Fig. 2(a)]. The spin-lattice relaxation rate is possibly much larger for the $\Gamma_{2,3}$ and $\Gamma_{5,6}$ than for the Γ_1 and Γ_4 levels.

B. NMR measurements

The longitudinal relaxation of the ^1H nuclear spin is dominated by the fluctuations of the magnetic moment of the iron(III) ions. In the case that each ^1H nuclear spin could relax independently from its neighboring protons simply due to the direct dipolar coupling with the spins of the iron ions, one would expect a broad distribution of relaxation times caused by the large number of magnetically unequal protons [72 in the $\text{Fe}_6(\text{tea})_6$ complex]. The experimental results reveal in general a monoexponential decay of the longitudinal magnetization. This is caused by diffusive processes due to mutual spin flips of neighboring protons, which establish a common spin temperature. Since the analysis of the averaging processes is complicated^{17,28} the following discussion of the ^1H T_1^{-1} rate is restricted to one proton, which is coupled via the dipolar interaction with the fluctuation spectrum of the iron(III) ions. Important conclusions can be drawn from the analysis of the fluctuation spectrum $f_{\text{NMR}}(\nu_0) = \int_{-\infty}^{+\infty} \langle F^+(\tau) F^-(0) \rangle \exp(+i2\pi\nu_0\tau) d\tau$, which leads to the longitudinal relaxation of the nuclear proton spins. $f_{\text{NMR}}(\nu_0)$ is calculated for the proton indicated by an asterisk in Fig. 1(a) (the shortest ^1H -Fe distance is 3.095 Å). The contour plots of $T_1^{-1}(\nu, B)$ for $B \perp c$, $T = 15$ K, $B < 5$ T and for $B \perp c$, $T = 3$ K in the field range of the first level crossing are shown in Figs. 10(a) and 10(b), respectively. The solid lines indicate the variation of the ^1H Larmor frequency with the magnetic

field strength $2\pi\nu_0 = \gamma_H B$. In contrast to the experimental results (Figs. 6 and 7), the largest T_1^{-1} rate in Fig. 10(a) is by a factor of 20 smaller than in Fig. 10(b). This results from the terms $D_0(i)s_i^\mp$ and $D_{\pm 2}(i)s_i^\pm$ in Eq. (3a), which contribute in the field range of the level crossing. It is interesting to note that the term $D_0(i)$ is not only important in the range of the level crossing, but enters also into the description of the transversal relaxation T_2^{-1} rate by the term $\frac{2}{3}D_0(i)s_i^\mp$ in F^\times [Eq. (3a)] which contributes to the zero-frequency fluctuations. The measured T_2^{-1} rates are indeed at least by a factor of 10 larger than the largest T_1^{-1} measured rates. A possible explanation for the reduced T_1^{-1} rate in the range of the level crossing is given below.

Figure 10(a) shows that transitions between excited spin states ($S=1, 2 \leftrightarrow 3$ and $S=2, 5 \leftrightarrow 6, 7 \leftrightarrow 8$) contribute to T_1^{-1} for small magnetic field strengths. The intensity of the $\nu=0$ contribution $m_0^{(\nu=0)}$ increases with increasing magnetic field strength and dominates the T_1^{-1} rate at 52 MHz. The width of the fluctuation spectrum increases slightly with the strength of the magnetic field. $\Delta\nu_{1/2} \approx 400$ MHz at $B = 1.2$ T and $\nu_0 = 52$ MHz seems to be large when compared with the ^1H Larmor frequency, but reasonable if $\Delta\nu_{1/2}$ is converted into an ESR linewidth ($\Delta B_{1/2} = 2\pi\Delta\nu_{1/2} / \gamma_S \approx 140$ G).

Figure 10(b) illustrates the fluctuation spectrum in the range of the level crossing around $B = 15$ T and $B \perp c$ calculated for $T = 3$ K. There are two peaks of the T_1^{-1} rate—one below and the other above $B_c = 15.02$ T. Figure 10(c) shows that the calculated magnitude of the T_1^{-1} peak above and below B_c is different. This results from the terms $D_0(i)s_i^\mp$ and $D_{\pm 2}(i)s_i^\pm$ in Eq. (3a) which dominate either on the left side or the right side of B_c , respectively. Asymmetric T_1^{-1} peaks which resemble our numerical results were recently observed for a Cr_8 ring.²⁹

The width $\Delta B_{1/2} \approx 240$ G [see Fig. 10(c)] of the calculated T_1^{-1} peak is by a factor of 10 smaller than the experimental value. It is interesting to note that the calculated $\Delta B_{1/2}$ is nevertheless in the range of the ESR linewidth discussed in Sec. IV A. Affronte *et al.*²⁵ proposed that a level anticrossing can effectively broaden the peak of the T_1^{-1} rate. A level anticrossing can be induced by the Dzyaloshinski-Moriya interaction [Hamiltonian Eq. (1e)], which has therefore been included into the Hamiltonian $\mathcal{H}_{\text{Fe}_6}$. Figures 11(a) and 11(b) show the influence of the DM interaction and the level anticrossing on the fluctuation spectrum around B_c , calculated with $D/k_B = 0.01$ and 0.02 K, respectively. It turns out that the level anticrossing induced by the DM interaction shifts the fluctuation spectrum of the iron ring already for small values of D out of the range of the ^1H Larmor frequency, without inducing a broadening of the T_1^{-1} peak. Although we cannot exclude the presence of a small DM interaction for the $\text{Fe}_6(\text{tea})_6$ system, we note that the DM interaction is not responsible for the broadening of the T_1^{-1} peak.

The calculated field value of the level crossing $B_c = 15.02$ T is smaller than the experimental value of 15.63 T. This cannot be attributed to an incorrect orientation of the crystal, since B_c is nearly independent of the angle $\angle(B, c)$ for perpendicular field orientation [$\approx \Delta B_c / \angle(B, c) = 0.005$ T/1 deg]. On the other hand, B_c depends critically

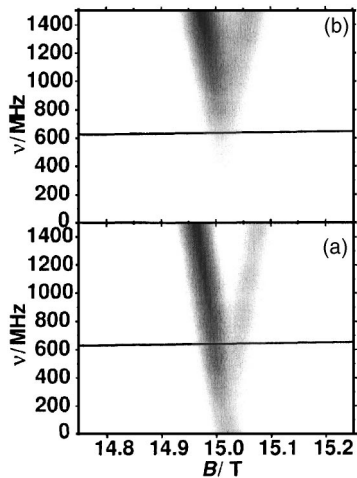


FIG. 11. Influence of the Dzialoshinski-Moriya interaction [Eq. (1e)] on $T_1^{-1}(\nu, B)$ calculated for $B \perp c$, $T = 3$ K in the field range of the first level crossing (black, high values of T_1^{-1} ; white, $T_1^{-1} = 0$). The variation of the ^1H Larmor frequency $\nu_0 = \gamma_B B / 2\pi$ is indicated by a solid line. $D/k_B =$ (a) 0.01, (b) 0.02 K.

on the exchange interaction J , with $\Delta B_c / \Delta |J| = 0.512$ T/K for perpendicular field orientation. $B_c = 15.63$ T indicates that the exchange interaction is stronger than $J/k_B = -31.5$ K, which was determined by static susceptibility measurements. The fit of B_c yields $J/k_B = -32.7 \pm 0.2$ K. The strong dependence of B_c on the exchange interaction J can also contribute to the width of the T_1^{-1} peak if there is a distribution of molecular J values, which might be caused by small differences of the molecular configurations at low temperatures. Due to the width $\Gamma = 0.2$ T of the T_1^{-1} peak (see Sec. III B), a width of $\Delta J/k_B \approx 0.4$ K can be expected for the corresponding distribution of exchange constants. This might be possible, since it is known that J depends critically on geometrical parameters (e.g., the relation between J and the bridging angle $\alpha_1 = \angle(\text{Fe-O-Fe})$ is J (K) $= -2.91\alpha_1$ (deg) $+ 276$,^{10(b)} so that $\Delta J/k_B \approx 0.4$ K would correspond to an angular variation of $\Delta\alpha_1 \approx 0.14^\circ$). In general, it can be expected that the six exchange constants of the iron(III) ring will be modified independently from each other, when there is a distortion of the molecular symmetry at low temperatures. The generalized exchange Hamiltonian $\mathcal{H}_{\text{ex}} = \sum_{i=1}^6 -J_{i,i+1} \vec{s}_i \vec{s}_{i+1}$ can, however, be decomposed into the six irreducible representations of the group 6 of the cyclic permutations of the indices i . The totally symmetric component transforming according to Γ_1 will replace the exchange Hamiltonian Eq. (1a), i.e., the exchange constant will be replaced by the average $\bar{J} = \frac{1}{6} \sum_{i=1}^6 J_{i,i+1}$, and the values of \bar{J} will scatter around J determined by B_c . Concerning the other components of \mathcal{H}_{ex} , only the component transforming like Γ_4 will influence the lowest spin states and induce a level anticrossing between the ground state $\Gamma_4(S=0)$ and the first excited state of $\Gamma_1(S=1)$ at the magnetic field determined by \bar{J} . As for the DM interaction, the fluctuation spectrum can be shifted out of the frequency range accessible by the ^1H Larmor frequency and the corresponding molecule will not contribute to the T_1^{-1} peak. This might explain why the T_1^{-1} rate is considerably

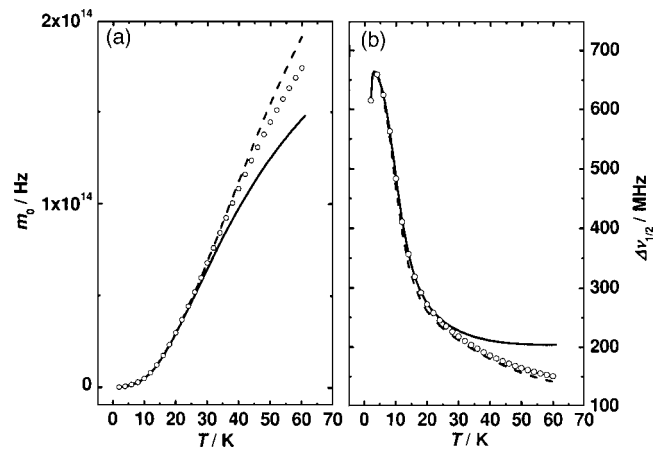


FIG. 12. Calculated temperature dependence of the moment $m_0^{(\nu=0)}$ and the half-width $\Delta\nu_{1/2}^{(\nu=0)} = \sqrt{m_2^{(\nu=0)}(2 \ln 2)}$ of the spectral density $f_{\text{NMR}}(\nu=0)$ calculated for $B = 1.2$ T and $B \perp c$. Solid lines and points: the calculation includes the lowest spin states up to $\Gamma_1(S=3)$ and $\Gamma_4(S=4)$, respectively. Dashed lines: all spin states shown in Fig. 2(a) are included.

smaller than expected and why there are—despite spin diffusion—fast and slowly relaxing components of the nuclear magnetization when T_1 is measured in the range of B_c [compare Fig. 7(b)]. The generalization of \mathcal{H}_{ex} will hardly be detected by ESR experiments since neither the totally symmetric nor the Γ_4 component will modify in first order the zero-field splitting of the spin states. The T_1^{-1} peak of the NMR experiment on the other hand will not reflect the Lorentzian shape of the spectral density $f_{\text{ESR}}(\nu)$ detected by the ESR experiment but the distribution of \bar{J} values within the crystal, which might be a Gaussian function. Finally, not only J but also the anisotropy parameter d can be modified by distortions of the molecular geometry. The relation between the anisotropy parameter d and geometrical parameters was discussed in Ref. 10(b) and it turns out that there exists a linear relation between d and a special rotation angle φ according to d (K) $= 0.0196\varphi$ (deg) $- 2.65$. This leads to the conclusion that the modification of d due to geometrical distortions is ~ 150 times smaller than the modification of J , and is therefore negligible. The fact that the T_1^{-1} peak is broadened whereas the broadening of the ESR lines remains within the expected range, although the ESR lines would be strongly influenced by a distribution of the d values, confirms that the modification of d due to geometrical distortions is indeed negligible.

Figure 12 shows the temperature dependence of the moment $m_0^{(\nu=0)}$ and the half-width $\Delta\nu_{1/2}^{(\nu=0)} = \sqrt{m_2^{(\nu=0)}(2 \ln 2)}$ of the $\nu=0$ resonance for $B \perp c$ and $B = 1.2$ T. We show separately the results of the calculation including the lowest spin states $S=0, 1, 2$, and 3 (solid lines), the spin states up to the first excited spin state $S=4$ (open circles), and all spin states that are shown in Fig. 2(a) (dashed lines). $m_0^{(\nu=0)}$ follows an activated temperature dependence [see the Appendix, Eq. (A1b)], whereas the width of the fluctuation spectrum $\Delta\nu_{1/2}^{(\nu=0)}$ is predicted to become smaller with increasing temperature since the contribution of the $S=1$ levels, which are important at low temperatures, is reduced at higher temperatures. The

inclusion of excited spin states leads to a reduced width of the spectral density for $T \geq 30$ K. The influence on the width of the spin states above the first excited $S=4$ levels is very small. Their influence on the intensity $m_0^{(\nu=0)}$ of the spectral density is, however, not negligible. These results predict a steep increase of the T_1 rate without a maximum at $T_{\max} \approx 40$ K [compare Fig. 6(b)]. There are two scenarios that can lead to an experimentally observed maximum of the T_1 rate in this temperature range. When the width $\Delta\nu_{1/2}^{(\nu=0)}$ of the fluctuations is smaller than predicted by the calculation, the ^1H Larmor frequency might become larger than $\Delta\nu_{1/2}^{(\nu=0)}(T)$ above a certain temperature, which would efficiently reduce the T_1 rate. However, the temperature of the resulting maximum would in this scenario depend critically on the ratio between ν_0 and $\Delta\nu_{1/2}^{(\nu=0)}$, while the experimental results of Lascialfari *et al.*^{4(a)} in the frequency range between 7 and 60 MHz reveal no frequency dependence of T_{\max} . Another possible explanation for the T_1 maximum would be that the spectral density $f_{\text{NMR}}(\nu_0)$ is broadened by the onset of spin-lattice relaxation as can be observed for the ESR transitions in the temperature range above $T \approx 35$ K (Fig. 5). This broadening effectively reduces the value of $f_{\text{NMR}}(\nu_0)$ at the ^1H Larmor frequency and leads to a maximum of the T_1 rate, which indicates the onset of strong spin-phonon interactions.

V. CONCLUSIONS

We have studied the spin dynamics of the cyclic iron(III) system $\text{Fe}_6(\text{tea})_6$ by ESR and ^1H NMR measurements. The spin Hamiltonian of the $\text{Fe}_6(\text{tea})_6$ molecule has been diagonalized and the eigenstates have been used to calculate the influence of the intermolecular dipolar interaction on the spectral densities, which determine the ESR lines and ^1H nuclear spin-lattice relaxation rate. The calculation is restricted to the second moment and neglects the contribution of inelastic processes to the width of the spectral density, which could be particularly important in the vicinity of the level crossing. Despite these limitations, it is shown that the calculation of the spectral density provides a valuable basis for the discussion of the experimental results.

The angular variation of the ESR linewidth and the temperature dependence below $T \leq 35$ K can be reasonably well be described by this approach. The steep increase of the ESR linewidth above $T \geq 35$ K indicates the onset of strong spin-phonon interactions which can be described in terms of the Orbach and Raman processes. The temperature-dependent measurements of the ^1H T_1^{-1} rate at 1.2 T reveal a maximum of the T_1^{-1} rate in the temperature range around 40 K. It might be that this maximum of the T_1^{-1} rate is also caused by the onset of spin-lattice relaxation. The ^1H T_1^{-1} rate measured at low temperatures in the field range between 12 and 17 T shows the characteristic peak at $B_c = 15.61$ due to the level crossing between the $S=0$ ground state and the first excited level of the $S=1$ state. The comparison of the experimental results with the analysis of the spin dynamics indicates that a distribution of molecular distortions leads to iron rings with different exchange constants J , which results in the large width of the peak and its Gaussian shape.

ACKNOWLEDGMENTS

This work was supported by the Deutsche Forschungsgemeinschaft (DFG) via Projects No. PI336/2-1,2 and No. PI336/4-1 and by the European Community via "Access to Research Infrastructure action of the Improving Human Potential Program." B.P. wishes to thank Professor E. Dormann for his support of the work.

APPENDIX

One way to calculate the influence of a perturbation on the resonances of the spectral density $f(\nu) = \int_{-\infty}^{\infty} \langle A(\tau)B(0) \rangle \exp(+i2\pi\nu\tau) d\tau$ is the so-called method of moments.¹⁹ The resonance lines are reconstructed by a small number of moments. It was pointed out by van Vleck that the Hamiltonian of the perturbation has to include only those terms that commute with the Hamiltonian of the unperturbed system. The truncated Hamiltonian of the perturbation is called secular and the remaining terms nonsecular. The method of moments can be applied when the mixing of the wave functions due to the perturbation is small and the resulting satellite resonances can be neglected. We take the Hamiltonian of the iron rings $\mathcal{H}_0 = \sum_{j=1}^N \mathcal{H}_{\text{Fe}_6}^{(j)}$ as the unperturbed Hamiltonian and the intermolecular dipolar coupling [Eq. (A4), see below] as the perturbation \mathcal{H}' . The method of moments can be safely applied since no satellite resonances due a perturbation could be detected in the ESR spectra of the iron ring systems. Pryce and Stevens showed by means of projection operators how the secular part can be constructed.³⁰ The intensity $m_0 = \int_{\text{around } \nu_0} f(\nu) d\nu$ of the resonance at $h\nu_0 = (E_n - E_{n'})$ is

$$m_0 = \frac{1}{Z^N} \text{Tr}[\exp(-P_n \mathcal{H}_0 P_n / k_B T) P_n A P_n' B]. \quad (\text{A1a})$$

P_n denotes the projection operators on the eigenstates $|n\rangle$ of the total unperturbed Hamiltonian \mathcal{H}_0 . Equation (A1a) can be easily calculated with the eigenstates and eigenfunctions of the individual cluster $\mathcal{H}_{\text{Fe}_6}^{(j)} |\mu\rangle = E_{\mu}^{(j)} |\mu\rangle$:

$$m_0 = \frac{1}{Z} \sum_{\mu, \mu'} \exp(-E_{\mu}^{(j)} / k_B T) \langle \mu | A^{(j)} | \mu' \rangle \langle \mu' | B^{(j)} | \mu \rangle, \quad (\text{A1b})$$

where $h\nu_0 = (E_{\mu}^{(j)} - E_{\mu'}^{(j)})$ and $Z = \sum_{\mu} \exp(-E_{\mu}^{(j)} / k_B T)$.

The first moment $m_1 = (1/m_0) \int (\nu - \nu_0) f(\nu) d\nu$ of the resonance at $h\nu_0 = (E_n - E_{n'})$ describes the frequency shift of the line due to the perturbation \mathcal{H}' ,

$$m_1 = \frac{1}{h m_0 Z^N} \text{Tr}[\exp(-P_n \mathcal{H}_0 P_n / k_B T) (P_n A P_n' \mathcal{H}' P_n' B - P_n \mathcal{H}' P_n' A P_n' B)], \quad (\text{A2})$$

and the second moment $m_2 = (1/m_0) \int (\nu - \nu_0)^2 f(\nu) d\nu$ becomes

$$m_2 = \frac{1}{h^2} \frac{1}{m_0 Z^N} \text{Tr}[\exp(-P_n \mathcal{H}_0 P_n / k_B T) \times (P_n A P_n' \mathcal{H}' P_n' \mathcal{H}' P_n' B + P_n \mathcal{H}' P_n' \mathcal{H}' P_n' A P_n' B - 2P_n A P_n' \mathcal{H}' P_n' B P_n' \mathcal{H}')] \quad (\text{A3})$$

m_1 and m_2 have been calculated by McMillan and Opechowski²⁰ and Zevin and Shanina²¹ in terms of the eigenvalues $E_\mu^{(j)}$ and eigenfunctions $|\mu\rangle$ of the unperturbed Hamiltonian. But the formulas are long and will therefore not be reproduced here.

The intermolecular dipolar interaction is determined by the crystal structure. It is therefore straightforward to calculate the influence of the intermolecular dipolar interaction on the spectral density $f(\nu)$ by the technique sketched above. The secular part of the intermolecular dipolar interaction be-

tween a central and the neighboring iron rings is given by

$$\mathcal{H}' = (g\mu_B)^2 \sum_{i=1}^6 \sum_{j \neq 1}^6 \sum_{k=1}^6 \frac{3}{2} (1 - 3 \cos^2 \Theta_{ik}^{(j)}) \frac{1}{(r_{ik}^{(j)})^3} \times \left(s_i^{(1)z} s_k^{(j)z} - \frac{1}{3} s_i^{(1)} s_k^{(j)} \right). \quad (\text{A4})$$

j denotes all the neighboring iron rings. $s_i^{(1)}$ and $s_k^{(j)}$ are the spins of the central and neighboring ring j , respectively. $r_{ik}^{(j)}$ denotes the distance between spin $s_i^{(1)}$ and $s_k^{(j)}$. $\Theta_{ik}^{(j)}$ denotes the angle between the vector $r_{ik}^{(j)}$ and the external magnetic field, which is oriented along z . All rings with the center to origin distance smaller than 25 Å were included into the calculation, namely, 28 rings around the central ring as shown in Fig. 1(b).

-
- ¹A. Caneschi, A. Cornia, A. C. Fabretti, S. Foner, D. Gatteschi, R. Grandi, and L. Schenetti, *Chem.-Eur. J.* **2**, 1379 (1996).
- ²A. Caneschi, M. Capaccioli, L. Cianchi, A. Cornia, F. DelGiallo, F. Pieralli, and G. Spina, *Hyperfine Interact.* **116**, 215 (1998).
- ³O. Waldmann, T. Guidi, S. Carretta, C. Mondelli, and A. L. Dearden *Phys. Rev. Lett.* **91**, 237202 (2003).
- ⁴(a) A. Lascialfari, D. Gatteschi, F. Borsa, and A. Cornia, *Phys. Rev. B* **55**, 14341 (1997); (b) A. Lascialfari, Z. H. Jang, F. Borsa, D. Gatteschi, and A. Cornia, *J. Appl. Phys.* **83**, 6946 (1998); (c) A. Lascialfari, D. Gatteschi, A. Cornia, U. Balucani, M. G. Pini, and A. Rettori, *Phys. Rev. B* **57**, 1115 (1998).
- ⁵D. Procissi, B. J. Suh, E. Micotti, A. Lascialfari, Y. Furukawa, and F. Borsa, *J. Magn. Magn. Mater.* **272-276**, 741 (2004); see also cond-mat/0404378 (unpublished); cond-mat/0404379 (unpublished).
- ⁶(a) A. Chiolero and D. Loss, *Phys. Rev. Lett.* **80**, 169 (1997); (b) F. Meier and D. Loss, *ibid.* **86**, 5373 (2001).
- ⁷O. Waldmann, *Europhys. Lett.* **60**, 302 (2002).
- ⁸A. Honecker, F. Meier, D. Loss, and B. Normand, *Eur. Phys. J. B* **27**, 487 (2002).
- ⁹O. Waldmann, C. Dobe, H. Mutka, A. Furrer, and H. U. Güdel, cond-mat/0410447 (unpublished).
- ¹⁰A. Cornia, A. G. M. Jansen, and M. Affronte, *Phys. Rev. B* **60**, 12177 (1999); O. Waldmann, R. Koch, S. Schromm, J. Schülein, P. Müller, I. Bernt, R. W. Saalfank, F. Hampel, and E. Balthes, *Inorg. Chem.* **40**, 2986 (2001); Y. Shapira and V. Bindilatti, *J. Appl. Phys.* **92**, 4155 (2002).
- ¹¹H. U. Güdel, in *Molecular Magnetism*, edited by E. Coronado *et al.* (Kluwer Academic Publishers, Dordrecht, 1996).
- ¹²(a) B. Pilawa, R. Desquiotz, M. T. Kelemen, M. Weickenmeier, and A. Geißelmann, *J. Magn. Magn. Mater.* **177-181**, 748 (1997); (b) B. Pilawa, I. Keilhauer, R. Bofinger, D. Marinov, S. Knorr, and A. Grupp, *Appl. Magn. Reson.* **21**, 527 (2001); (c) B. Pilawa, I. Keilhauer, G. Fischer, S. Knorr, J. Rahmer, and A. Grupp, *Eur. Phys. J. B* **33**, 321 (2003).
- ¹³A. Geißelmann, Diploma work, Universität Karlsruhe, 1996.
- ¹⁴G. F. Koster, J. O. Dimmock, R. G. Wheeler, and H. Satz, *Properties of the Thirty-Two Point Groups* (MIT Press, Cambridge, MA, 1969). The application of the permutation operation T leads to $T|\Gamma_1\rangle = +|\Gamma_1\rangle$, $T|\Gamma_4\rangle = -|\Gamma_4\rangle$, $T|\Gamma_{2,3}\rangle = \omega^{\mp 4}|\Gamma_{2,3}\rangle$, and $T|\Gamma_{5,6}\rangle = \omega^{\pm 2}|\Gamma_{5,6}\rangle$, with $\omega = \exp(i\pi/6)$.
- ¹⁵T. Moriya, *Phys. Rev.* **120**, 91 (1960).
- ¹⁶R. M. White, *Quantum Theory of Magnetism* (McGraw-Hill, New York, 1970).
- ¹⁷A. Abragam, *The Principles of Nuclear Magnetism* (Clarendon Press, Oxford, 1961).
- ¹⁸T. Moriya, *Prog. Theor. Phys.* **16**, 23 (1956).
- ¹⁹J. H. van Vleck, *Phys. Rev.* **74**, 1168 (1948).
- ²⁰M. McMillan and W. Opechowski, *Can. J. Phys.* **38**, 1168 (1960).
- ²¹V. Zevin and B. Shanina, *Ukr. Fiz. Zh.* **11**, 1089 (1966).
- ²²R. Kubo and K. Tomita, *J. Phys. Soc. Jpn.* **9**, 888 (1954).
- ²³M.-J. Julien, Z. H. Jang, A. Lascialfari, F. Borsa, F. Horvatić, M. Caneschi, and D. Gatteschi, *Phys. Rev. Lett.* **83**, 227 (1999).
- ²⁴A. Cornia, A. Fort, M. G. Pini, and A. Rettori, *Europhys. Lett.* **50**, 88 (2000).
- ²⁵M. Affronte, A. Cornia, A. Lascialfari, F. Borsa, D. Gatteschi, J. Hinderer, M. Horvatić, A. G. M. Jansen, and M.-H. Julien, *Phys. Rev. Lett.* **88**, 167201 (2002).
- ²⁶R. Orbach, *Proc. R. Soc. London, Ser. A* **264**, 458 (1961).
- ²⁷G. E. Pake, *J. Chem. Phys.* **16**, 327 (1948).
- ²⁸T.-T. Phua, B. J. Beaudry, D. T. Peterson, D. R. Torgeson, R. G. Barnes, M. Belhoul, G. A. Styles, and E. F. W. Seymour, *Phys. Rev. B* **28**, 6227 (1983).
- ²⁹A. Lascialfari, F. Borsa, M.-H. Julien, E. Micottic, Y. Furukawa, Z. H. Jang, A. Cornia, D. Gatteschi, M. Horvatić, and J. van Slageren, *J. Magn. Magn. Mater.* **272-276**, 1042 (2004).
- ³⁰M. H. L. Pryce and K. W. H. Stevens, *Proc. Phys. Soc., London, Sect. A* **63**, 36 (1950).